MODELLING OF VIBRATION AND MODAL PROPERTIES OF ELECTRIC LOCOMOTIVE DRIVE

Olimjon Ahmedov*, Vladimír Zeman*, Miroslav Byrtus*

The article provides a method of mathematical modelling of the dynamic properties of the electric locomotive wheelset drive. The linkage of the traction motor by means of the rotor pinion gear with the gear of wheelset drive is considered. The impact of couplings and operation conditions on the dynamic properties is studied. The method of decomposition into subsystems is applied for derivation of mathematical model of an interconnected system. This model is used for the calculation of modal values and also for investigating the forced vibration excited by pulsation moments of the asynchronous traction motor. The method is applied to a particular drive of the locomotive SKODA 109E.

Keywords: *railway vehicle, wheelset drive, modal analysis, modal values, pulsation moments, dynamic response*

1. Introduction

In cooperation with SKODA TRANSPORTATION a.s. and within the frame of research project 1M0519 Research centre of Rail Vehicles, it has been required to test the dynamic load of wheelset drive of the 109E electric locomotive in an extreme state of stress caused by short-circuit torque and pulsation torque in one of the individual drives. Dynamic response of wheelset drive components at the moment of the sudden short-circuit in one asynchronous traction motor [1] has been investigated under consideration of a rigid rotor of the traction motor supported on rigid bearings [2, 3]. For the analysis of vibration excited by high-frequency pulsation moments [4] of the traction motor it is necessary to respect a flexible rotor supported on flexible bearings in a vibrating stator of the traction motor. In order to model the dynamic response, it is necessary to develop a methodology by which a proper mathematical model of the electric locomotive wheelset drive is formulated. Its computer program representation allows faults simulation and focuses on the modelling of dynamic drive effects. Simulations demonstrate that the dynamic response caused by sources generated in the traction engine depends on the operating parameters of the locomotive at the moment just before the perturbation. The individual wheelset drive vibrates dominantly, where the torque pulsation moments resonate with eigen frequencies of the wheelset drive. The torsional excitation and very flexible disk clutch (DC) between driven gear (G) and hollow shaft (H) embracing the wheelset axle (Fig. 1) afford separation of the system on spatially vibrating driving part (in front of DC) and torsional vibrating driven part (hollow shaft and wheelset) of the individual wheelset drive.

* Ing. O. Ahmedov, prof. Ing. V. Zeman, DrSc., Ing. M. Byrtus, Ph.D., Department of Mechanics, University of West Bohemia, Univerzitní 22, 30614 Plzeň, Czech Republic

2. Modelling of subsystems

To model the vibration and dynamic loading, the wheelset drive (Fig. 1) was decomposed into five subsystems :

– Rotor of traction motor (RM) with a pinion gear (P) in the nodal point 16 without the bearings,
– Gear (G) with the hub lug and the driving part of disc clutch (DC),
– Stator of traction motor (S) fixed with gearbox,
– Hollow shaft (H) embracing the wheelset axle and the driven part of disc clutch and driving part of gear clutch (GC),
– Wheelset (W) with the driven gear clutch part.

The general location of the subsystems in the coordinate system displayed right is described by generalized coordinates summarized in Tab. 1.

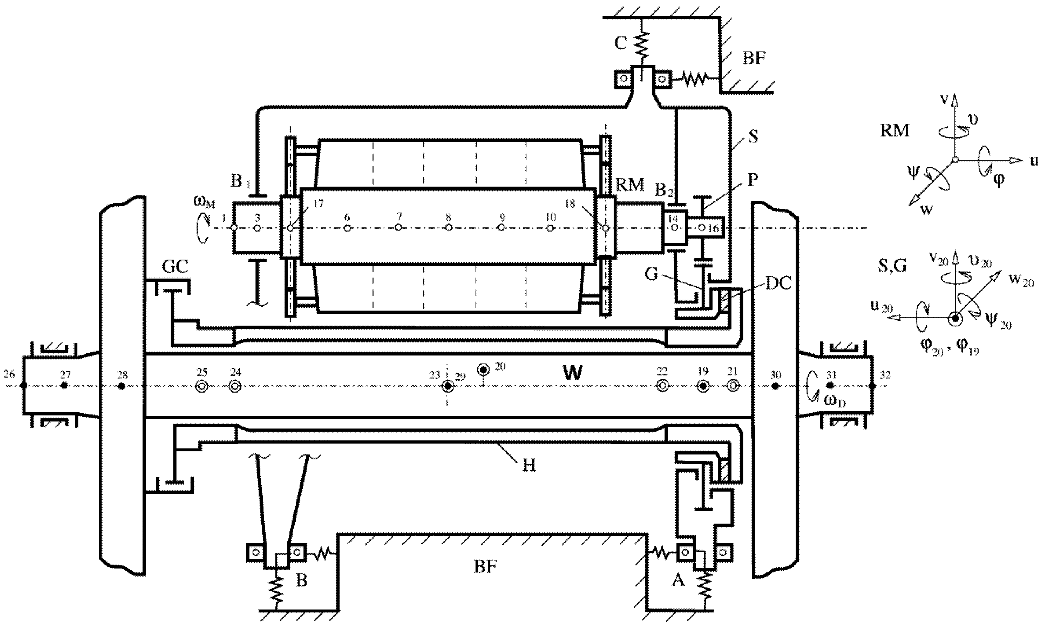

Fig.1: Scheme of individual wheelset drive and coordinate systems

Subsystem	Degrees of freedom	The order of the generalized coordinates	Generalized coordinates
Rotor of motor (RM)	108	1–108	$u_1, v_1, w_1, \varphi_1, \vartheta_1, \psi_1, \ldots, u_{18}, v_{18}, w_{18}, \varphi_{18}, \vartheta_{18}, \psi_{18}$
Gear (G)	1	109	φ_{19}
Stator (S)	6	110–115	$u_{20}, v_{20}, w_{20}, \varphi_{20}, \vartheta_{20}, \psi_{20}$
Hollow shaft (H)	5	116–120	$\varphi_{21}, \ldots, \varphi_{25}$
Wheelset (W)	7	121–127	$\varphi_{26}, \ldots, \varphi_{32}$

Tab.1: Generalized coordinate of subsystems

2.1. Rotor of the motor (RM)

Rotor of the traction motor ML4550/6 (Fig. 2) was modelled in [5] provided the spatial oscillations of its components. The engine model was added to the pinion in the 16th node (see Fig. 3). For the purposes of separate modelling of linkages between subsystems the bearings in nodes 3 and 14 are removed. The rotor is characterized by a flexible shaft with mounted packet of sheet metals which are equipped with parallel copper bars connected to short-circuit rings. The shaft is modelled as spatially vibrating one dimensional continuum discretized into 15 finite elements with 16 nodes. The one dimensional beam elements have been used because the shaft diameter is relatively small with respect to the shaft length. The sheet metal packet with copper bars passing through is modelled by five rigid bodies connected to the shaft nodes 6 and 10 [5]. The model is characterized by mass $\mathbf{M}_{\mathrm{RM}}$, stiffness $\mathbf{K}_{\mathrm{RM}}$ and gyroscopic $\mathbf{G}_{\mathrm{RM}}$ matrices of order 108.

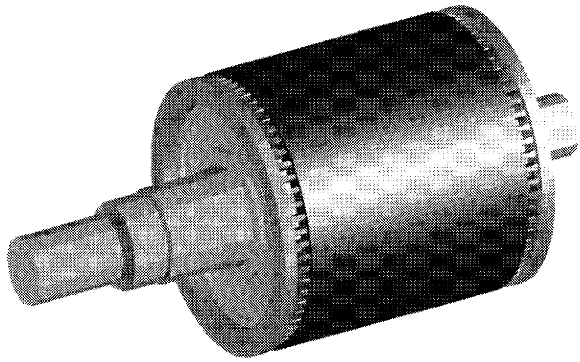

Fig.2: Rotor of a squirrel cage motor (visualization)

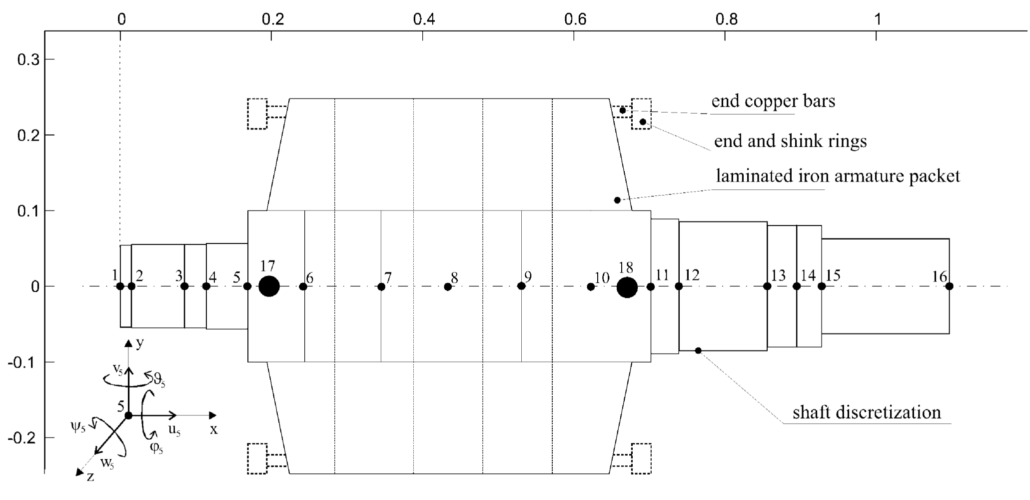

Fig.3: Scheme of rotor model

2.2. Stator of the traction motor (S)

We assume a torsion displacement φ_{19} of the gear wheel inside the spatially vibrating gearbox, which is fixed with stator of traction motor. Hence, the second subsystem (see Tab. 1) is displayed in the global mass matrix by torsion moment of inertia I_{G} and mass concentrated in centre of gravity is associated with stator. It is considered that the stator with gearbox is a rigid body with centre of gravity in point 20 (see Fig. 1). In configuration space

$$\mathbf{q}_{\mathrm{S}} = [u_{20}, v_{20}, w_{20}, \varphi_{20}, \vartheta_{20}, \psi_{20}] \ , \tag{1}$$

the stator is characterized by mass matrix

$$\mathbf{M}_{\mathrm{S}} = \begin{bmatrix} m_{\mathrm{S}}\,\mathbf{E} & \mathbf{0} \\ \mathbf{0} & \mathbf{I}_{\mathrm{S}} \end{bmatrix} \in R^{6,6} \tag{2}$$

of order 6, where m_{S} is mass, $\mathbf{E}$ unit matrix and $\mathbf{I}_{\mathrm{S}}$ is inertia matrix in cordinate system marked in the Fig. 1 by S with coordinate basic origin in stator centre of gravity (point 20). The stator with gearbox is connected to the bogie frame by silent blocks with centres of elasticity A, B, C. We assume that the bogie frame is in its static equilibrium.

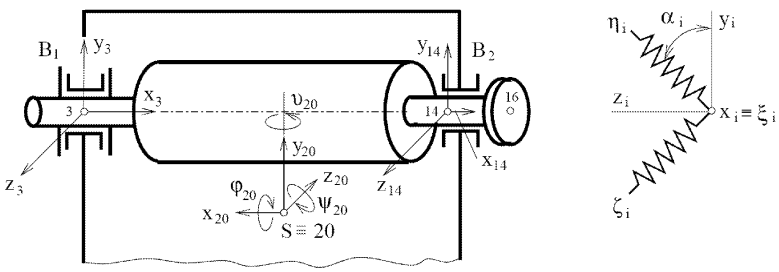

Fig.4: Scheme of the couplings between rotor and stator of the traction motor

2.3. Gear (G), hollow shaft (H), wheelsets (W)

We assume torsional oscillations of gear (G) superimposed at spatial motion of its axis rigidly supported in the gearbox and purely torsional oscillating, hollow shaft and wheelset, described by angular displacements, $\varphi_{19}, \dots, \varphi_{32}$ (see Fig. 1). Torsional vibrating subsystem consisting of the hollow shaft (H) and wheelsets (W) is characterized by a submatrices $\mathbf{M}_{\mathrm{T}}, \mathbf{K}_{\mathrm{T}} \in R^{12,12}$.

The matrices of the mutually isolated subsystems are included in the global matrices of the individual wheelset drive in the form of the block-diagonal structures

$$\mathbf{M} = \mathrm{diag}[\mathbf{M}_{\mathrm{RM}}, I_{\mathrm{G}}, \mathbf{M}_{\mathrm{S}}, \mathbf{M}_{\mathrm{T}}] \ , \qquad \mathbf{K} = \mathrm{diag}[\mathbf{K}_{\mathrm{RM}}, 0, \mathbf{K}_{\mathrm{S,BF}}, \mathbf{K}_{\mathrm{T}}] \tag{3}$$

according to the global vector of generalized coordinates

$$\mathbf{q} = [\mathbf{q}_{\mathrm{RM}}, \varphi_{19}, \mathbf{q}_{\mathrm{S}}, \mathbf{q}_{\mathrm{T}}]^{\mathrm{T}} \in R^{127} \ , \tag{4}$$

where the matrices with the subscript T correspond to torsional subsystem and the matrix $\mathbf{K}_{\mathrm{S,BF}}$ expresses stiffness elastic supports (silentblocks) A, B, C (see Fig. 1) on the bogie frame.

3. Stiffness matrices of couplings between subsystems

Coupling stiffness matrices between subsystems are derived in configuration space defined in (4). In comparison with previous models in [3], [6], the couplings between rotor and stator of the traction motor and between pinion gear and gearbox wheel are now totally changed.

Hence, we will introduce theirs derivation. Moreover, the rolling-element bearing stiffness is linearized relative to static load which is given by an operational state of the running locomotive defined by longitudinal creepage s_0 of the wheels, forward velocity v and by vertical wheel force N_0. The dynamic components of the forces which are transmitted by bearings change not much because the torsional vibration is dominant.

The shaft of the rotor is supported on two roller bearings B_1 and B_2, where the left one is the radial-axial (Fig. 4). Principal directions η_i, ζ_i of radial bearing stiffnesses k_{η_i}, k_{ζ_i} include angle α_i with corresponding frame axes y_i, z_i ($i = 3, 14$). The deformation energy of the bearings is given by following form

$$E_\mathrm{B} = \frac{1}{2}\,\mathbf{d}_3^\mathrm{T}\,\mathbf{K}_3\,\mathbf{d}_3 + \frac{1}{2}\,\mathbf{d}_{14}^\mathrm{T}\,\mathbf{K}_{14}\,\mathbf{d}_{14}\ , \tag{5}$$

where $\mathbf{K}_i = \mathrm{diag}[k_{\xi_i}, k_{\eta_i}, k_{\zeta_i}]$ are diagonal bearing stiffness matrices, whereas $k_{\xi_{14}} = 0$. The transfer of the bearing centres caused by stator vibration (1) in the coordinate system of the rotor is described by the vector $\mathbf{T}_\mathrm{S,RM}\,(\mathbf{u}_{20} + \mathbf{R}_i^\mathrm{T}\,\boldsymbol{\varphi}_{20})$, where $\mathbf{T}_\mathrm{S,RM} = \mathrm{diag}(-1, 1, -1)$ and components of the vector $\mathbf{u}_{20} = [u_{20}, v_{20}, w_{20}]^\mathrm{T}$ represent displacement of centre gravity of stator and the vector $\boldsymbol{\varphi}_{20} = [\varphi_{20}, \vartheta_{20}, \psi_{20}]^\mathrm{T}$ describes angle displacements of the stator. Operators $\mathbf{R}_i$ of cross product are defined by radius vectors of bearing centres in coordinate system x_{20}, y_{20}, z_{20}. Deformation vectors of the bearings in coordinate system ξ_i, η_i, ζ_i of the main stiffness directions of the bearings can be expressed as

$$\mathbf{d}_i = \mathbf{T}_i\,[\mathbf{u}_i - \mathbf{T}_\mathrm{S,RM}\,(\mathbf{u}_{20} + \mathbf{R}_i^\mathrm{T}\,\boldsymbol{\varphi}_{20})]\ ,\quad i = 3, 14\ , \tag{6}$$

where

$$\mathbf{T}_i = \begin{bmatrix} 1 & 0 & 0 \\ 0 & \cos\alpha_i & \sin\alpha_i \\ 0 & -\sin\alpha_i & \cos\alpha_i \end{bmatrix}\ ,\quad i = 3, 14\ . \tag{7}$$

The stiffness matrix results from the identity

$$\frac{\partial E_\mathrm{B}}{\partial \mathbf{q}} = \mathbf{K}_\mathrm{RM,S}\,\mathbf{q}$$

and in the compressed from is

$$\bar{\mathbf{K}}_\mathrm{RM,S} = \begin{bmatrix} \mathbf{T}_3^\mathrm{T}\,\mathbf{K}_3\,\mathbf{T}_3 & \mathbf{0} & -\mathbf{T}_3^\mathrm{T}\,\mathbf{K}_3\,\mathbf{T}_{3,20} \\ \mathbf{0} & \mathbf{T}_{14}^\mathrm{T}\,\mathbf{K}_{14}\,\mathbf{T}_{14} & -\mathbf{T}_{14}^\mathrm{T}\,\mathbf{K}_{14}\,\mathbf{T}_{14,20} \\ -\mathbf{T}_{3,20}^\mathrm{T}\,\mathbf{K}_3\,\mathbf{T}_3 & -\mathbf{T}_{14,20}^\mathrm{T}\,\mathbf{K}_{14}\,\mathbf{T}_{14} & \mathbf{T}_{3,20}^\mathrm{T}\,\mathbf{K}_3\,\mathbf{T}_{3,20} + \mathbf{T}_{14}^\mathrm{T}\,\mathbf{K}_{14}\,\mathbf{T}_{14,20} \end{bmatrix}\ , \tag{8}$$

where

$$\mathbf{T}_{i,20} = \mathbf{T}_i\,\mathbf{T}_\mathrm{S,RM}\,[\mathbf{E}_3, \mathbf{R}_i^\mathrm{T}] \in R^{3,6}\ ,\quad i = 3, 14\ . \tag{9}$$

The block in (8) are localized in the full stiffness matrix $\mathbf{K}_\mathrm{RM,S} \in R^{127,127}$ in accordance with subvectors $\mathbf{u}_3$, $\mathbf{u}_{14}$ and $\mathbf{q}_{20}$ in the global vector $\mathbf{q}$ of generalized coordinates.

The general configuration of spur helical gears (Fig. 5) is described by pinion gear and gearbox wheel vectors of displacements $\mathbf{q}_i = [u_i, v_i, w_i, \varphi_i, \vartheta_i, \psi_i]^\mathrm{T}$, ($i = 16, 19$). In the coordinate system ξ, η, ζ, the vector of relative deviation of the central interaction gearing point can be expressed in the form

$$(\mathbf{d})_{\xi\eta\zeta} = \begin{bmatrix} (v_{16} - v_{19})\,\cos\gamma + (w_{16} - w_{19})\,\sin\gamma - r_\mathrm{P}\,\varphi_{16} + r_\mathrm{G}\,\varphi_{19} \\ -(v_{16} - v_{19})\,\sin\gamma + (w_{16} + w_{19})\,\cos\gamma \\ (u_{16} + u_{19}) + r_\mathrm{P}\,\cos\gamma\,\vartheta_{16} + r_\mathrm{G}\,\cos\gamma\,\vartheta_{19} + r_\mathrm{P}\,\sin\gamma\,\psi_{16} - r_\mathrm{G}\,\sin\gamma\,\psi_{19} \end{bmatrix}\ , \tag{10}$$

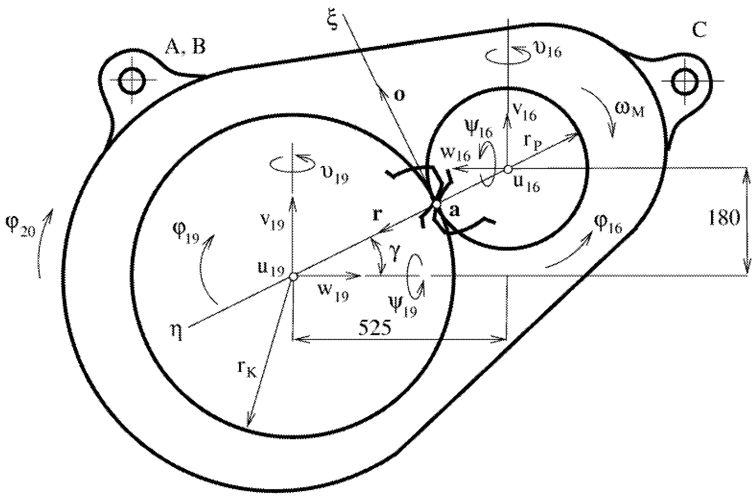

Fig.5: Scheme of a gearing coupling

where r_{P} is rolling of the radius of the driving pinion gear (driven gearbox wheel r_{G}) and γ is angle of position. The gearing deformation is given by vector $(\mathbf{d})_{\xi\eta\zeta}$ projection to normal line of the tooth faces [7]

$$d_{\mathrm{n}} = \mathbf{e}_n^{\mathrm{T}}\,(\mathbf{d})_{\xi\eta\zeta} = [\cos\alpha\,\cos\beta, \sin\alpha, \cos\alpha\,\sin\beta]\,(\mathbf{d})_{\xi\eta\zeta}\ , \tag{11}$$

where α is normal pressure angle and β is angle of inclination of the teeth. In accordance with (10) and (11) the gearing deformation is

$$d_{\mathrm{n}} = \boldsymbol{\delta}_{16}^{\mathrm{T}}\,\mathbf{q}_{16} + \boldsymbol{\delta}_{19}^{\mathrm{T}}\,\mathbf{q}_{19}\ , \tag{12}$$

where vectors of geometrical parameters of the gear pair are expressed as

$$\boldsymbol{\delta}_{16} = \begin{bmatrix} \cos\alpha\,\sin\beta \\ \cos\alpha\,\cos\beta\,\cos\gamma - \sin\alpha\,\sin\gamma \\ \cos\alpha\,\cos\beta\,\sin\gamma + \sin\alpha\,\cos\gamma \\ -r_{\mathrm{P}}\,\cos\alpha\,\cos\beta \\ r_{\mathrm{P}}\,\cos\alpha\,\sin\beta\,\cos\gamma \\ r_{\mathrm{P}}\,\cos\alpha\,\sin\beta\,\sin\gamma \end{bmatrix}, \quad \boldsymbol{\delta}_{19} = \begin{bmatrix} \cos\alpha\,\sin\beta \\ -\cos\alpha\,\cos\beta\,\cos\gamma + \sin\alpha\,\sin\gamma \\ \cos\alpha\,\cos\beta\,\sin\gamma + \sin\alpha\,\cos\gamma \\ r_{\mathrm{G}}\,\cos\alpha\,\cos\beta \\ r_{\mathrm{G}}\,\cos\alpha\,\sin\beta\,\cos\gamma \\ -r_{\mathrm{G}}\,\cos\alpha\,\sin\beta\,\sin\gamma \end{bmatrix}. \tag{13}$$

The displacement vector $\mathbf{q}_{19}$ of the gearbox wheel can be expressed by its torsional angular displacement φ_{19} and gearbox displacements as

$$\mathbf{q}_{19} = \mathbf{T}_{19,20}\,\mathbf{q}_{20} + [0,0,0,\varphi_{19},0,0]^{\mathrm{T}}\ , \tag{14}$$

where transformation matrix

$$\mathbf{T}_{19,20} = \begin{bmatrix} 1 & 0 & 0 & 0 & z_k & -y_k \\ 0 & 1 & 0 & -z_k & 0 & x_k \\ 0 & 0 & 1 & y_k & -x_k & 0 \\ 0 & 0 & 0 & 0 & 0 & 0 \\ 0 & 0 & 0 & 0 & 1 & 0 \\ 0 & 0 & 0 & 0 & 0 & 1 \end{bmatrix}$$

is defined by coordinates x_k, y_k, z_k of the nodal point 19 in the space x_{20}, y_{20}, z_{20}. According to (12) and (14) the gearing deformation is

$$d_{\mathrm{n}} = \boldsymbol{\delta}_{16}^{\mathrm{T}}\,\mathbf{q}_{16} + \boldsymbol{\delta}_{19}^{\mathrm{T}}\,\mathbf{T}_{19,20}\,\mathbf{q}_{20} + r_{\mathrm{G}}\,\cos\alpha\,\cos\beta\,\varphi_{19}\ . \tag{15}$$

Under the condition of uninterrupted gear mesh and main stiffness k_{G} of gearing in normal direction, the stiffness gear coupling matrix results form identity

$$\frac{\partial E_{\mathrm{d}}}{\partial \mathbf{q}} = \mathbf{K}_{\mathrm{P,G}}\,\mathbf{q}\ ,$$

where $E_{\mathrm{d}} = k_{\mathrm{G}}\,d_{\mathrm{n}}^2/2$ is deformation energy of the gear coupling. This matrix in the compressed form is

$$\bar{\mathbf{K}}_{\mathrm{P,G}} = k_{\mathrm{G}} \begin{bmatrix} \boldsymbol{\delta}_{16}\,\boldsymbol{\delta}_{16}^{\mathrm{T}} & R_{\mathrm{G}}\,\boldsymbol{\delta}_{16} & \boldsymbol{\delta}_{16}\,\boldsymbol{\delta}_{19}^{\mathrm{T}}\,\mathbf{T}_{19,20} \\ R_{\mathrm{G}}\,\boldsymbol{\delta}_{16}^{\mathrm{T}} & R_{\mathrm{G}}^2 & R_{\mathrm{G}}\,\boldsymbol{\delta}_{19}^{\mathrm{T}}\,\mathbf{T}_{19,20} \\ \mathbf{T}_{19,20}^{\mathrm{T}}\,\boldsymbol{\delta}_{19}\,\boldsymbol{\delta}_{16}^{\mathrm{T}} & R_{\mathrm{G}}\,\mathbf{T}_{19,20}^{\mathrm{T}}\,\boldsymbol{\delta}_{19} & \mathbf{T}_{19,20}^{\mathrm{T}}\,\boldsymbol{\delta}_{19}\,\boldsymbol{\delta}_{19}^{\mathrm{T}}\,\mathbf{T}_{19,20} \end{bmatrix}\ , \tag{16}$$

where $R_{\mathrm{G}} = r_{\mathrm{G}}\,\cos\alpha\,\sin\beta$. The block matrices in (16) are localized in the full stiffness matrix $\mathbf{K}_{\mathrm{P,G}} \in R^{127,127}$ in accordance with subvector $\mathbf{q}_{16}$, angular displacement φ_{19} and subvector $\mathbf{q}_{20}$ in the global vector $\mathbf{q}$ of generalized coordinates.

4. Mathematical model of the individual wheelset drive

Mathematical model of individual wheelset drive excited by pulsation moments of traction motor is derived by Lagrange's equations in generalized coordinates $\mathbf{q}(t)$ representing drive component displacements from static equilibrium of the moving vehicle on a geometrically perfect straight track under the operational conditions given by the longitudinal creepage s_0 of both wheels, electric locomotive velocity v [km/h] and vertical wheel forces N_0 [N]. Conservative model leaves out the creep forces in contact of the rails with the wheels has the form resulting from isolated subsystems and coupling stiffness matrices between subsystems and can be written as

$$\mathbf{M}\,\ddot{\mathbf{q}}(t) + (\mathbf{K} + \mathbf{K}_{\mathrm{RM,S}} + \mathbf{K}_{\mathrm{P,G}} + \mathbf{K}_{\mathrm{DC}})\,\mathbf{q}(t) = \mathbf{0}\ . \tag{17}$$

Matrix $\mathbf{K}_{\mathrm{DC}}$ expresses the stiffness disc clutch between gearbox wheel and hollow shaft.

Creep forces in contact of wheels with the rails are expressed by longitudinal adhesion forces $T_{i\,\mathrm{ad}}$ and create adhesion $M_{i\,\mathrm{ad}}$ moments. Their form can be expressed as (the index i marks nodes in which the wheels are fixed)

$$T_{i\,\mathrm{ad}} = \mu(s_i, v)\,N_0\ , \qquad M_{i\,\mathrm{ad}} = \mu(s_i, v)\,N_0\,r\ , \tag{18}$$

where N_0 is the normal force, r is wheel radius and $\mu(s_0, v)$ is coefficient of adhesion analytically expressed in [8]. Longitudinal creepage of the wheels is

$$s_i = s_0 + \frac{r\,\dot{\varphi}_i}{v}\,3.6\ , \qquad s_0 = \frac{3.6\,r\,\omega_{\mathrm{W}} - v}{v}\ ,$$

where v is forward locomotive velocity in [km/h] and s_0 is longitudinal creepage before perturbance. The coefficient of adhesion is expressed in linearized form

$$\mu(s_i, v) = \mu_0 + \left[\frac{\partial \mu}{\partial s_i}\right]_{s_i = s_0} (s - s_0)\ , \tag{19}$$

which corresponds to the moment of adhesion

$$M_{i\,\mathrm{ad}} = M(s_0, v) + b(s_0, v)\, \dot{\varphi}_i \ , \tag{20}$$

where

$$M(s_0, v) = \mu(s_0, v)\, N_0\, r \qquad \text{and} \qquad b(s_0, v) = \left[\frac{\partial \mu}{\partial s_i}\right]_{s_i = s_0} (s - s_0)\, \frac{N_0\, r^2}{v}\, 3.6 \ .$$

Linearized vector of adhesion moments in the form

$$\mathbf{f}_i = -b(s_0, v)\, \dot{\mathbf{q}}_i \ , \quad i = 28, 30 \tag{21}$$

complements conservative drive model (17) on the right side. A packet of sheets in the model of the rotor is replaced by five discs mounted on the shaft at nodes 6 to 10 (Fig. 3). Pulsating torque is evenly distributed to the packet of sheets. The vector representing the pulsation moments can be written in complex form

$$\begin{aligned} \mathbf{f}(t) &= \sum_k \mathbf{f}_k\, \mathrm{e}^{2\pi\, f_k\, t} \ , \\ \mathbf{f}_k &= \frac{1}{5}\, M(s_0, v)\, \eta_k\, [\dots, 1, \dots, 1, \dots, 1, \dots, 1, \dots, 1, \dots, 5, \dots]^{\mathrm{T}} \ , \end{aligned} \tag{22}$$

where $\mathbf{f}_k$ is the k-th excitation vector amplitudes with the excitation frequency f_k in Hz and digits 1 (digit 5) are localized on the positions corresponding to torsional displacement of the shaft nodal points 6 to 10 of the rotor (torsional displacements φ_{20} of the stator).

Excitation frequencies of pulsation moments and their amplitudes are adopted from the research report [4]. The values are listed in Tab. 2, where η_k is k-th relative amplitude of k-th component of torque pulsation M_k and $M(s_0, v)$ is the nominal torque before perturbance.

k	1	2	3	4	5
f_k [Hz]	663	939	1602	2265	2541
$\eta_k = M_k/M(s_0, v)$	0.15	0.1	0.276	0.008	0.075

Tab.2: Excitation frequency and amplitude of pulsed moments

The comprehensive model of individual drive, including the influence of adhesion moments in contact of wheels and rails, the impact of control on the engine torque characteristic determined by its inclination b_{E} and pulsation excitation of the traction motor torque has the form

$$\mathbf{M}\, \ddot{\mathbf{q}}(t) + (\omega_0\, \mathbf{G} + \mathbf{B}(s_0, v))\, \dot{\mathbf{q}}(t) + (\mathbf{K} + \mathbf{K}_{\mathrm{RM,S}} + \mathbf{K}_{\mathrm{P,G}} + \mathbf{K}_{\mathrm{DC}})\, \mathbf{q}(t) = \mathbf{f}(t) \ , \tag{23}$$

where

$$\mathbf{G} = \mathrm{diag}[\mathbf{G}_{\mathrm{RM}}, 0, \mathbf{0}, \mathbf{0}] \ , \quad \mathbf{B}(s_0, v) = \mathrm{diag}[\mathbf{B}_{\mathrm{RM}}, 0, \mathbf{B}_{\mathrm{S}}, \mathbf{B}_{\mathrm{ad}}(s_0, v)] \ .$$

The rotor damping matrix and adhesion properties are in diagonal form

$$\begin{aligned} \mathbf{B}_{\mathrm{RM}} &= \frac{1}{5}\, \mathrm{diag}(\dots, b_{\mathrm{E}}, \dots, b_{\mathrm{E}}, \dots, b_{\mathrm{E}}, \dots, b_{\mathrm{E}}, \dots, b_{\mathrm{E}}, \dots) \ , \\ \mathbf{B}_{\mathrm{ad}}(s_0, v) &= \mathrm{diag}(\dots, b(s_0, v), \dots, b(s_0, v), \dots) \qquad \text{and} \\ \mathbf{B}_{\mathrm{S}} &= \mathrm{diag}(0, 0, 0, b_{\mathrm{E}}, 0, 0) \ . \end{aligned} \tag{24}$$

Localization of matrix nonzero elements in $\mathbf{B}_{\mathrm{ad}}(s_0, v)$ corresponds to torsional deflections of wheels fixed on the axle wheelset.

5. Modal analysis of the individual wheelset drive

For illustration, Table 3 contains the first 10 natural frequencies f_v of conservative model (17), natural values of the model (24), damping factors defined by $-\alpha_v/|\lambda_v|$ and includes the corresponding mode shape characteristics of the wheelset drive for operational parameters $s_0 = 0.002$, $v = 200\,\mathrm{km/h}$ and $N = 10^5\,\mathrm{N}$.

v	Model (17) f_v [Hz]	Model (24) $\lambda_v = \alpha_v \pm \mathrm{i}\,\beta_v$ [Hz]	D_v	Characteristics of mode shapes
1	0	$0 \pm \mathrm{i}\,0$	0	torsion with no deformation
2	4.07	$-1.55 \pm \mathrm{i}\,0$	1.0	torsion drive with large deformation of disc clutch
3	27.16	$-2.0\mathrm{e}{-03} \pm \mathrm{i}\,24.92$	8.19e−05	yaw and lateral deformations RM and S
4	35.07	$-4.8\mathrm{e}{-03} \pm \mathrm{i}\,35.91$	1.36e−04	roll RM and S and vertical deformations end copper bars
5	48.97	$-27.49 \pm \mathrm{i}\,40.51$	5.6e−01	torsion DC and twisting of W
6	55.15	$-12.7\mathrm{e}{-04} \pm \mathrm{i}\,55.10$	2.32e−05	transverse vibrations RM and S
7	71.27	$-1.93\mathrm{e}{-02} \pm \mathrm{i}\,65.63$	2.9e−04	longitudinal vibrations RM and S
8	97.32	$-34.3\mathrm{e}{-02} \pm \mathrm{i}\,97.67$	3.5e−03	yaw of RM and P, pitch G
9	117.30	$-3.36\mathrm{e}{-02} \pm \mathrm{i}\,115.1$	2.92e−04	lateral of RM
10	123.60	$-3.2\mathrm{e}{-01} \pm \mathrm{i}\,120.46$	2.69e−03	roll of P and pitch G

Tab.3: Modal values of the individual drive

Dynamic gearing deformation (relative motion of gear teeth in normal line of the tooth faces) corresponding to particular mode shapes (Fig. 6) is important in terms of dynamic load of gearing.

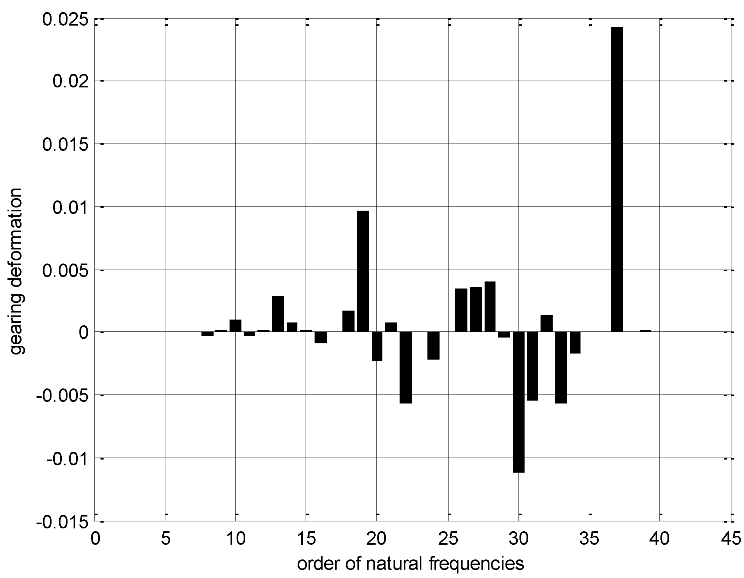

Fig.6:. Dynamic gearing deformation

6. Steady dynamic response caused by pulsation moments

Steady vibration of the wheelset drive excited by pulsation moments $\mathbf{f}(t)$ is expressed by particular solution of motion equations (24) in the complex form

$$\tilde{\mathbf{q}}(t) = \sum_{k=1}^{5} \tilde{\mathbf{q}}_k \, \mathrm{e}^{\omega_k \, t} \ , \qquad \omega_k = 2 \, \pi \, f_k \ , \tag{26}$$

where complex amplitude vectors of displacements are

$$\tilde{\mathbf{q}}_k = \left\{ -\mathbf{M} \, \omega_k^2 + \mathrm{i} \, \omega_k \, (\omega_0 \, \mathbf{G} + \mathbf{B}(s_0, v)) + (\mathbf{K} + \mathbf{K}_{\mathrm{RM,S}} + \mathbf{K}_{\mathrm{P,G}} + \mathbf{K}_{\mathrm{DC}}) \right\}^{-1} \mathbf{f}_k \ . \tag{27}$$

Real displacements can be expressed as

$$\mathbf{q}(t) = \mathrm{Re}\{\tilde{\mathbf{q}}(t)\} = \sum_{k=1}^{5} (\mathrm{Re}\{\tilde{\mathbf{q}}\} \, \cos \omega_k t - \mathrm{Im}\{\tilde{\mathbf{q}}\} \, \sin \omega_k t) \ . \tag{28}$$

As an illustration the amplitudes of the force transmitted by gearing for two longitudinal creepage $s_0 = 0.002$ and $s_0 = 0.005$ and for locomotive velocity $v = 200\,\mathrm{km/h}$ and vertical wheel forces $N = 10^5\,\mathrm{N}$ are presented in Fig. 7. The time behaviour of this force in interval $t \in \langle 0, 0.01 \rangle$ [s] is presented in Fig. 8.

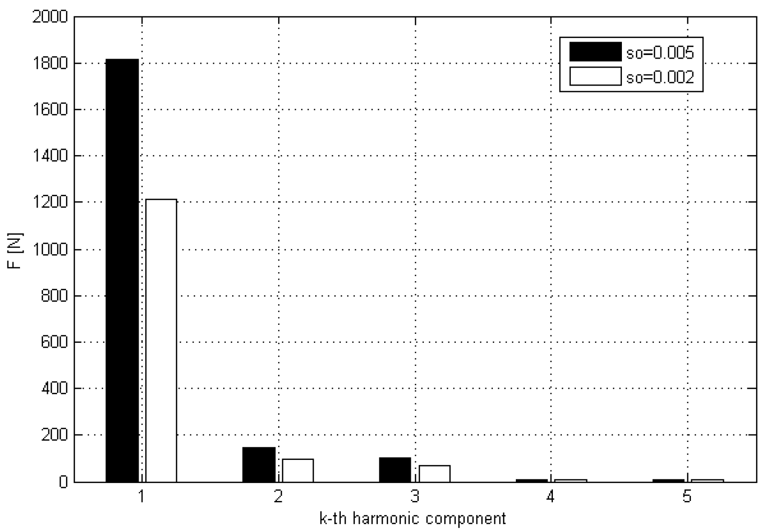

Fig. 7: Amplitudes of force transmitted by gearing excited by harmonic components of pulsating moment

7. Conclusions

The paper presents the method of mathematical modelling of the individual wheelset drive vibration of the electric locomotive caused by pulsation moments of the asynchronous traction motor. The derived linearized model and developed software in MATLAB code, expressed in perturbance coordinates with respect to static equilibrium (without pulsation

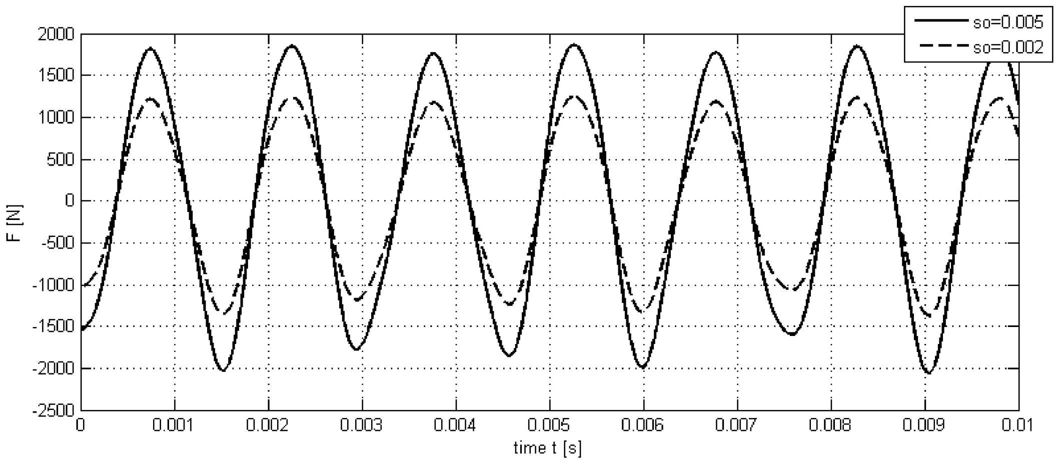

Fig.8: Time course of force transmitted by gearing

moments) of the moving locomotive on a geometrically ideal straight track, allows to investigate the possible resonant states caused by harmonic sources of excitation. For gear and pinion gears such resonances are dangerous when the first harmonic component of pulsating moment of traction motor resonates with natural frequencies up f_{17} to f_{19}, four harmonic component with frequency f_{33} and fifth harmonic with frequency f_{37}.

The developed software enables graphically record the time behaviour of the arbitrary generalized coordinate of the force transmitted by gearing for the arbitrary operational parameters of the locomotive expressed by the longitudinal creepage, locomotive velocity and vertical wheel forces using analytically defined creep characteristics. The dynamic response caused by pulsation moments depends especially on longitudinal creepage. In a close future, the derived wheelset drive model will be used for simulation of vibration and dynamical loading of drives components caused by kinematic transmission error of gearing.

Acknowledgements

The authors thank the student grant SGS-2010-046 at the University of West Bohemia and the project MSMT 1M0519 – Research Centre of Rail Vehicles for financial support.

References

[1] Dvořák P.: Calculated values of the short-circuit moment in the air-spase of the traction motor ML 4550 K/6, Documentation of ŠKODA EKECTRIC a.s., Plzeň, 2009 (in Czech)

[2] Zeman V., Hlaváč Z., Byrtus M.: Dynamic load of the vehicle bogie components of the electric locomotive 109E caused by short-circuit traction motor moment, Research report No. VZ č. F10-01/2010, VCKV, ZČU Plzeň, 2011 (in Czech)

[3] Zeman V., Hlavač Z.: Dynamic wheelset drive load of the railway vehicle caused by short-circuit motor moment, Applied and Computational Mechanics, Volume 3, No. 2, p. 423–434, Plzeň, 2009

[4] Bartoš V., Janda M.: Pulsationg torque of the asynchronous traction motor caused by inharmonious feeding, Research report of the project MPO ČR-2A-2TP-1/139, ZČU Plzeň, 2008 (in Czech)

[5] Hajžman M., Byrtus M., Zeman V.: Development of the Basic Dynamical Model of a Squirrel Cage Motor, Engineering Mechanics, Vol. 17, 2010, No. 3/4, p. 225–235

[6] Byrtus M., Zeman V., Hlavač Z.: Modelling and modal properties of an individual wheelset drive of a railway vehicle, Sborník 18. Mezinárodné konferencie Súčasné problemy v kolajových vozidlách – PRORAIL, Žilina, 2007

[7] Byrtus M., Zeman V.: On modeling and vibration of gear drives influenced by nonlinear couplings, Mechanism and Machine Theory, Vol. 46 (2011), No. 3, pp. 375–397

[8] Čáp J.: Some aspects of uniform comment of adhesion mechanism, Proceeding of VŠCHT Pardubice works, 1993, pp. 26–35 (in Czech)

Received in editor's office: July 7, 2011
Approved for publishing: June 20, 2012